

Research Article

Cite this article: Yang Z, Yang M, Sisson R, Li Y, Liang J (2022). Machine learning model to predict tensile properties of annealed Ti6Al4V parts prepared by selective laser melting. *Artificial Intelligence for Engineering Design, Analysis and Manufacturing* **36**, e30, 1–13. <https://doi.org/10.1017/S0890060422000117>

Received: 8 November 2021

Revised: 6 May 2022

Accepted: 18 May 2022


Key words:

annealing; artificial neural network; selective laser melting; tensile properties; Ti-6Al-4V

Author for correspondence:

Jianyu Liang,
E-mail: jjianyl@wpi.edu

Machine learning model to predict tensile properties of annealed Ti6Al4V parts prepared by selective laser melting

Zhaotong Yang¹, Mei Yang¹, Richard Sisson¹, Yanhua Li² and Jianyu Liang¹ 

¹Department of Mechanical and Materials Engineering, Worcester Polytechnic Institute, 100 Institute Road, Worcester, MA 01609, USA and ²Department of Computer Science, Worcester Polytechnic Institute, 100 Institute Road, Worcester, MA 01609, USA

Abstract

In this work, an artificial neural network model is established to understand the relationship among the tensile properties of as-printed Ti6Al4V parts, annealing parameters, and the tensile properties of annealed Ti6Al4V parts. The database was established by collecting published reports on the annealing treatment of selective laser melting (SLM) Ti6Al4V, from 2006 to 2020. Using the established model, it is possible to prescribe annealing parameters and predict properties after annealing for SLM Ti-6Al-4V parts with high confidence. The model shows high accuracy in the prediction of yield strength (YS) and ultimate tensile strength (UTS). It is found that the YS and UTS are sensitive to the annealing parameters, including temperature and holding time. The YS and UTS are also sensitive to initial YS and UTS of as-printed parts. The model suggests that an annealing process of the holding time of fewer than 4 h and the holding temperature lower than 850°C is desirable for as-printed Ti6Al4V parts to reach the YS required by the ASTM standard. By studying the collected data of microstructure and tensile properties of annealed Ti6Al4V, a new Hall-Petch relationship is proposed to correlate grain size and YS for annealed SLM Ti6Al4V parts in this work. The prediction of strain to failure shows lower accuracy compared with the predictions of YS and UTS due to the large scattering of the experimental data collected from the published reports.

Introduction

Titanium alloys are widely used as advanced structural materials, due to their desirable properties such as high strength to weight ratio, biocompatibility, corrosion resistance, desirable fracture toughness, and good fatigue performance (Donachie, 2000; Tamilselvi *et al.*, 2006; Banerjee and Williams, 2013; Lin *et al.*, 2017). However, Titanium alloys are difficult to machine because of the low thermal conductivity of the alloys (Qian, 2010). They are not easy to cast, either due to the high reactivity of liquid Titanium or the high melting point of Titanium alloy. Consequently, Titanium parts are frequently acquired by forging process. However, forging has issues such as long process time and a large fraction of raw material being wasted (Luo *et al.*, 2010; Tirelli *et al.*, 2015). Thus, the additive manufacturing (AM) technology, which enables the fabrication of Titanium parts with high geometric freedom, high accuracy, and great complexity, became attractive (Frazier, 2014; Herzog *et al.*, 2016). Among AM technologies, selective laser melting (SLM) is a laser-based powder-bed melting process. It uses a precisely controlled, high-energy laser to fabricate 3D parts from a CAD file, in a layer-by-layer fashion (Carpenter Technical Datasheet Titanium Alloy Ti 6Al-4V; Herzog *et al.*, 2016). Among all Titanium alloys, Ti6Al4V accounts for more than 50% of total usage (Carpenter Technical Datasheet Titanium Alloy Ti 6Al-4V). Ti6Al4V is also the most extensively studied Titanium alloy for AM process (Qian *et al.*, 2016). Many studies have investigated fabricating Ti6Al4V parts by the SLM method (Simonelli *et al.*, 2012; Rafi *et al.*, 2013; Kumar *et al.*, 2018).

The mechanical properties of Ti6Al4V parts prepared by the SLM process is the key factor in determining quality and applicability. It is well known that the nonequilibrium phase of martensite forms in the as-printed sample, instead of the more desirable equilibrium $\alpha+\beta$ phases. This is due to the high-temperature gradient and the high solidification rate in the melting pool. This microstructure results in rather low elongation (EL) and a low strain-hardening rate of as-printed Ti6Al4V samples (Ahmed and Rack, 1998; Ducato *et al.*, 2013; Huang *et al.*, 2016; Barriobero-Vila *et al.*, 2017). It has also been widely reported that there was a high residual stress in as-printed Ti6Al4V (Simonelli *et al.*, 2014; Yadroitsev and Yadroitsava, 2015; Yadroitsava *et al.*, 2015; Parry *et al.*, 2016). Furthermore, it was found that the laser scan strategy had a significant influence on the direction of grain growth, and led to an anisotropic tensile property in as-printed parts. In order to resolve these problems,

annealing is widely applied to as-printed parts. Multiple studies have been conducted to examine the annealing process and investigate the effect of annealing for Ti6Al4V, including reaction kinetics (Stefansson *et al.*, 2002; Semiatin *et al.*, 2005), phase morphology (Katzarov *et al.*, 2002; Semiatin *et al.*, 2003), corrosion resistance (Xu *et al.*, 2017; Etefagh *et al.*, 2019), microstructure, and mechanical properties under different annealing conditions (Wang *et al.*, 2016; Bilgin *et al.*, 2017). However, there is still a need to build a model that can predict the tensile properties of the post-treatment Ti6Al4V parts prepared by the SLM process, based on the tensile properties of the as-printed parts and the annealing parameters. According to Shi *et al.*, it is well recognized that the relation between microstructure and properties of Ti6Al4V is nonlinear and interactive. So, it is challenging to describe this connection as a mathematical relationship (Shi *et al.*, 2015). In the recent years, the artificial neural network (ANN) has emerged as a powerful tool to solve multivariable nonlinear modeling problems in different subject fields. For example, ANN has been successfully employed to predict the tensile properties of wrought titanium alloys, using composition and fabricating features as inputs (Kar *et al.*, 2006; Glavicic and Venkatesh, 2014; Ghamarian *et al.*, 2016; Hayes *et al.*, 2017).

As shown in Figure 1, the goal of this work is to establish an effective model through an ANN algorithm, one that uses the mechanical properties of as-printed Ti6Al4V parts prepared by SLM and annealing parameters as inputs and uses the tensile properties of post-annealing parts as outputs. The software package, Tensorflow, was adopted to build the model. Data of the annealing treatment and tensile properties of Ti6Al4V parts were collected from publications and reports between 2006 and

2020. Using data from different research groups across this extensive time span to build the model reduces potential bias due to machine-to-machine and process-to-process variation. The results of this study show that final tensile properties depend on the annealing conditions such as holding time and temperature, as well as on the initial tensile properties of as-printed parts. In addition, this study proposes a Hall-Petch relation with a new σ_0 of 767 MPa and a new Hall-Petch coefficient of 191 MPa $\mu\text{m}^{1/2}$ for powder-bed fusion Ti6Al4V. By using the established ANN model, the tensile properties of annealed Ti6Al4V parts fabricated by SLM can be predicted with high accuracy.

Data and methods

Artificial neural network

This work used the ANN algorithm to build the relationships among mechanical properties of as-printed Ti-6Al-4V prepared by the SLM process, annealing parameters, and the final mechanical properties of heat-treated parts. As shown in Figure 2, the ANN algorithm has three sections: an input layer, two hidden layers, and an output layer. There are different amounts of artificial neurons in each layer. All the neurons work in the same mathematical pattern (Theodoridis, 2015).

The activation function used in this study was the ReLU function, as shown in Eq. (1):

$$O = \begin{cases} z, & z \geq 0, \\ 0, & z < 0, \end{cases} \quad (1)$$

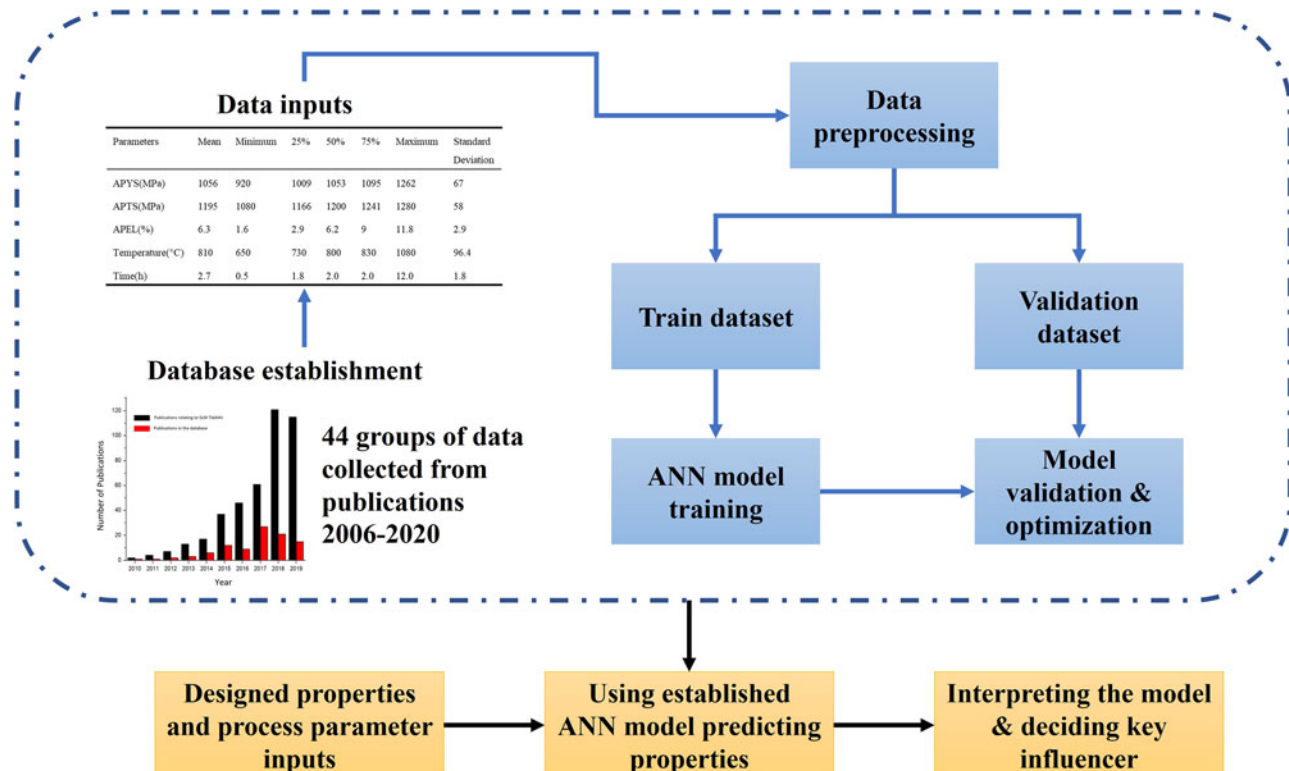


Fig. 1. Graphical abstract of this work.

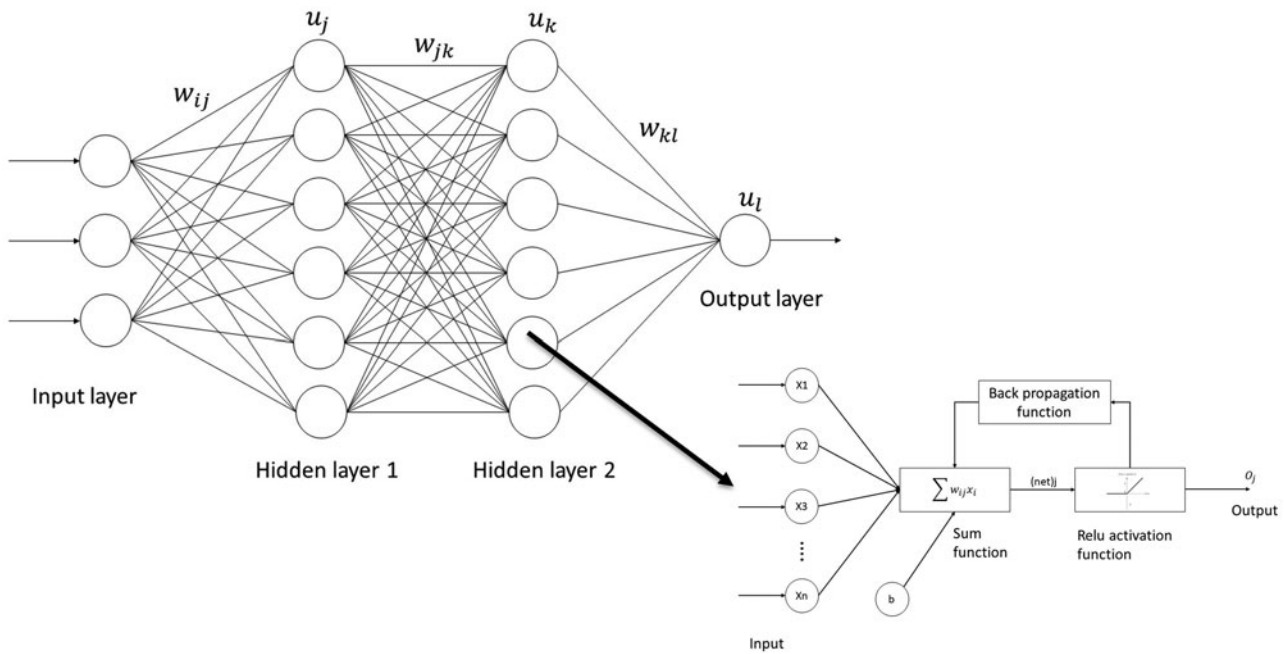


Fig. 2. Schematic architecture of the artificial neural network.

where O is the output of the neuron and z is the input of each neuron. Equation (2) is the cost function for the ANN:

$$C = \frac{1}{2m} \sum_{j=1}^m (O_j - y_j)^2, \tag{2}$$

where m is the total value of data series and y is the target value given by the dataset. The new w and b values after one iteration were obtained by Eqs (3) and (4):

$$w^i = w^i - \alpha \frac{\partial C}{\partial w^i}, \tag{3}$$

$$b = b - \alpha \frac{\partial C}{\partial b}. \tag{4}$$

Iteration was conducted for selected times, in order to reduce the number of w and b , until the model reached a global minimum.

The ANN model is a feed-forward and back-propagation algorithm, which can be expressed by Eqs (5)–(8):

$$dW^{[l]} = \frac{\partial L}{\partial W^{[l]}} = \frac{1}{m} dZ^{[l]} dA^{[l-1]} T, \tag{5}$$

$$db^{[l]} = \frac{\partial L}{\partial b^{[l]}} = \frac{1}{m} \sum_{i=1}^m dZ^{[l(i)]}, \tag{6}$$

$$dA^{[l-1]} = \frac{\partial L}{\partial A^{[l-1]}} W^{[l]T} dZ^{[l]}, \tag{7}$$

$$dZ^{[l]} = dA^{[l]} * g'(Z^{[l]}), \tag{8}$$

where the dw , db , dA , and dZ are derivatives of cost function, m is the value of examples, L is the cost function, and l is the vector of the layers.

Before modeling, a data normalization process was performed to reduce the variance of data scale in different input features. To improve the model’s accuracy, normalization is an essential step and is widely used in data pre-processing for machine learning and model-fitting (Alam, 2020). A standardization (Z-score normalization) was used in this study, as shown in Eq. (9):

$$X_{\text{new}} = \frac{x - \mu}{\sigma}, \tag{9}$$

where μ is the mean value, and σ is a standard deviation.

The number of neurons in the input layer was decided by the inputs. Each model produced one specific output (YS, or UTS, or EL). Table 1 summarizes the number of parameters in the ANN model: 448 parameters in hidden layer 1, 4160 parameters in hidden layer 2, and 65 parameters in the output layer. A RMSprop

Table 1. The values of parameters in the ANN model

Parameters	ANN
Number of neurons in the input layer	6
Number of hidden layers	2
Number of neurons in the first hidden layer	64
Number of neurons in the second hidden layer	64
Number of neurons in the output layer	1
Learning cycle	1000
Total parameters	4673
RMSprop factor	0.001
Activation function	ReLU

function was added to adjust the learning rate, which could reduce the size of the gradient steps, to dampen the oscillations (Gandhi, 2018). It is represented by Eqs (10) and (11):

$$E[g^2]_t = \beta E[g^2]_{t-1} + (1 - \beta) \left(\frac{\partial C}{\partial w} \right)^2, \quad (10)$$

$$w_t = w_{t-1} - \frac{n}{\sqrt{E[g^2]}} \frac{\partial C}{\partial w}, \quad (11)$$

where $E[g]$ is the moving average of the squared gradients, dC/dw is the gradient of the cost function, β is the moving average parameter, and n is the learning rate. The feed-forward, back-propagation was conducted 1000 times (epochs). These parameters were chosen because they resulted in high accuracy of prediction results without excessive computational complexity.

Data

The data used in this study were collected from published reports on heat-treatment studies of powder-bed fusion (SLM and electron beam melting) Ti6Al4V from 2006 to 2020, using Google Scholar, Science Direct, Research Gate, and Springer. The data from SLM studies were used to build the ANN model. The data from both SLM and electron beam melting (EBM) studies were used to update the Hall-Petch relation.

The data entries of the SLM studies that were used in the ANN modeling are summarized in Table 2. Forty-four groups of collected data were used to build and test the model for the annealing treatment of SLM Ti6Al4V samples. The data were collected from 16 published studies that conducted tensile property tests for both as-printed and annealed Ti6Al4V samples and provided detailed annealing parameters, including holding time, annealing temperature, and cooling method. The database consisted of tensile properties (YS, UTS, and elongation) of SLM Ti6Al4V before and after annealing, the microstructure information, and the annealing process parameters (temperature, holding time, and cooling method). The cooling method was labeled with different numbers that represent different cooling methods. In most of the studies that contributed data to this study, the cooling method for annealing was found to be furnace cooling under protective gas. So, the cooling method was not included in this model as a variable.

Before the training process, the dataset was randomly divided into a training set and a testing set. The training set was used to train the model, and the testing set was used to test the accuracy of the model. For the training set, 80% of data were used, and the remaining 20% served as the testing set. Dividing the database

into training and testing sets is a well-established method for the ANN process (Alpaydin, 2020).

Results and discussion

Yield strength

The established model was first used to predict the YS after annealing of Ti6Al4V prepared by SLM.

The mean absolute error (MAE) signifies the difference between prediction and experimental value, and in addition to accuracy, was used as a main indicator of the model's performance. The MAE was defined by Eq. (12):

$$MAE = \frac{\sum_{i=1}^n |y_i - x_i|}{n} = \frac{\sum_{i=1}^n |e_i|}{n}, \quad (12)$$

where y_i is the prediction result, x_i is the experimental data, and n is the quantity of the data. The prediction error e_i is the difference between the experimental value and the predicted value for a data point. A small MAE value indicates high consistency between the prediction by the model and the experimental data. In the modeling process, the MAEs of the training set and testing set were obtained and compared. The error calculated from the training set is referred to as train error, and the error from the set is referred to as the validation error. The results of the train error represent the performance of the model in the learning process, and the results of the validation error reflect the model's ability to generalize. The mean square error (MSE) was also used to show accuracy; MSE is the mean of the squares of prediction error e_i .

As shown in Figure 3a, during the learning process, the MAE dropped drastically between 0 epochs (iterations) and 400 epochs for both train error and validation error. The validation error decreased to 20 MPa at 620 epochs and stayed at this level until the learning process ended. At 1000 epochs, the final MAE of all data (including both training set and testing set) was found to be very small (31.2 MPa), which indicated a desirable learning result from the modeling process. As shown in Figure 3b, MSE for both the training set and the validation set gradually approached a small number during the learning process, which also indicated the high accuracy of prediction results.

Figure 4a shows the prediction results versus experimental results. The black line indicates that the prediction results are equal to the experimental data. The blue points are defined by the predicted results in the y -axis and the corresponding experimental data in the x -axis. The closer the blue points to the black line, the higher the accuracy of the model. Figure 4a clearly shows that the prediction results are in good agreement with the experimental data. Figure 4b shows the distribution of the prediction error within certain ranges. In previous studies on the

Table 2. The range of the input parameters in the ANN model

Parameters	Mean	Minimum	25%	50%	75%	Maximum	Standard Deviation
APYS (MPa)	1056	920	1009	1053	1095	1262	67
APTS (MPa)	1195	1080	1166	1200	1241	1280	58
APEL (%)	6.3	1.6	2.9	6.2	9	11.8	2.9
Temperature (°C)	810	650	730	800	830	1080	96.4
Time (h)	2.7	0.5	1.8	2.0	2.0	12.0	1.8

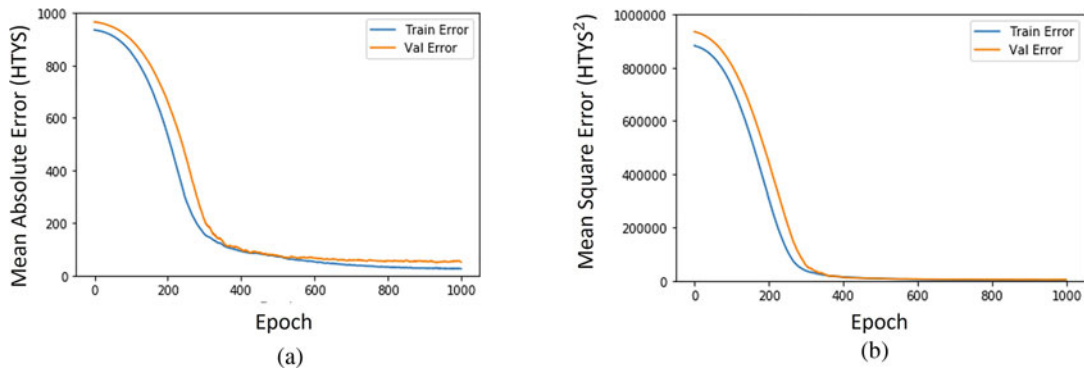


Fig. 3. (a) Mean absolute error (MAE) and (b) mean square error (MSE) in the training process for predicting yield strength of annealed SLM Ti6Al4V.

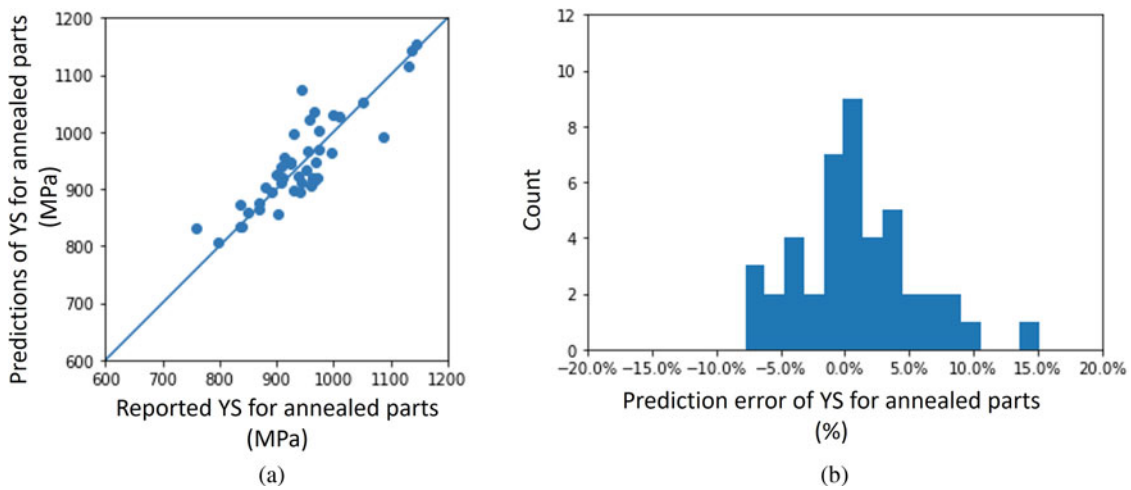


Fig. 4. (a) The correlation of the reported and predicted yield strength (YS) values of annealed AM Ti6Al4V, in the ANN model and (b) the distribution of YS prediction error in each range.

simulation and prediction of properties of Ti6Al4V, the acceptable error range was defined as 10% (Malinov *et al.*, 2001). In this study, a 5% error range was used as the measure of the model’s accuracy. As shown in Figure 4b, 88.6% of the predicted values using the full data (including both training set and testing set) were within the 5% error range, which confirmed a satisfactory accuracy of the model. The accuracy number of the model is described by Eq. (13):

$$\text{accuracy number} = 100\% - 100\% * \frac{\sum_{i=1}^n (|y_i - x_i|/x_i)}{n}, \quad (13)$$

where x_i is the experimental data, y_i is the prediction result, and n is the quantity of the data. The accuracy number of the ANN model in predicting yield strength for annealed SLM Ti6Al4V parts was found to be 96.7%. Thus, in summary, the model was successfully established with high accuracy.

The model was then used to reveal the correlation between the mechanical properties and the annealing process parameters. As shown in tables in Figure 5a,b, six groups of the data, which contained as-printed YS, as-printed UTS, as-printed elongation, and annealing temperature or annealing holding time, were used as inputs to the model. The inputs of the first three groups were YS of as-printed samples (APYS), UTS of as-printed samples

(APTS), and elongation of as-printed samples (APEL) at the 25 percentile, 50 percentile, and 75 percentile of corresponding data ranges in Table 2. In Group 1, 25 percentile of YS for as-printed samples (APYS); 25 percentile of UTS for as-printed samples (APTS); and 75 percentile of elongation for as-printed samples (APEL) from Table 2 were used as inputs. In group 2, the 50 percentile of YS (APYS), UTS (APTS), and El (APEL) for as-printed samples in Table 2 were used. In Group 3, 75 percentile of YS for as-printed samples (APYS); 75 percentile of UTS for as-printed samples (APTS), and 25 percentile of elongation for as-printed samples (APEL) from Table 2 were used as inputs. The other three groups of data were randomly selected. The predictions of the YS of annealed parts as a function of time and temperature are shown in Figure 5a,b. As shown in Figure 5a, in general, the YS decreased with the increase in holding time: it decreased from 1011–837 MPa to 883–711 MPa, when the holding time increased from 1 to 4 h. Figure 5b reveals that the YS also decreased with the increase in holding temperature in the range of 650–1000°C. It is well known that long holding time and high holding temperature promote grain growth and result in low YS for annealed parts. Ter Haar and Becker (2018) found that the median α lamellar width increased from 1.5 to 8 μm when the annealing time was increased from 0.5 to 4 h. Vrancken *et al.* (2012) observed that the α - β morphology was

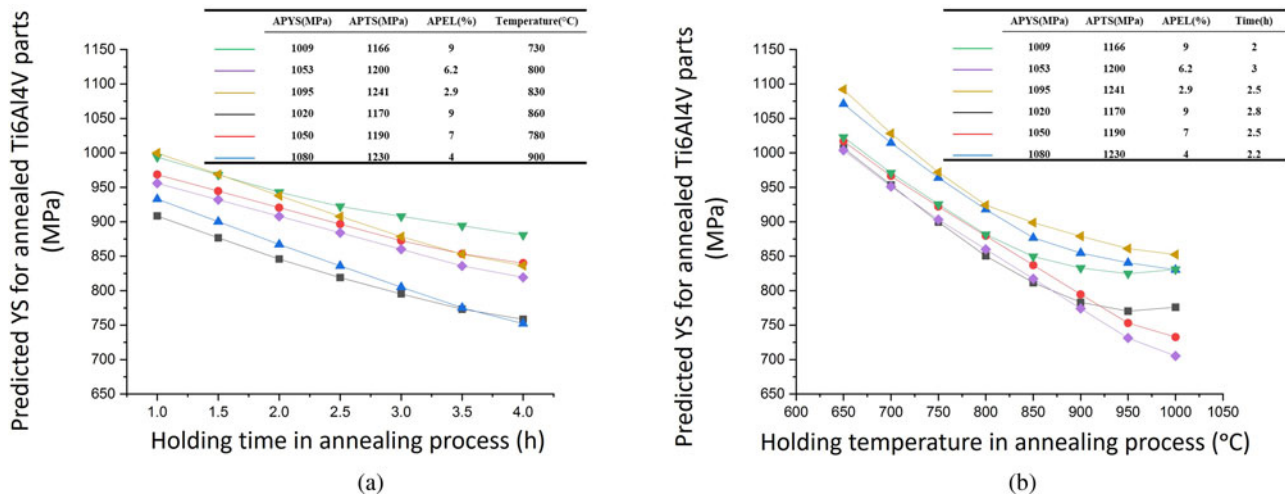


Fig. 5. The influence of heat treatment parameters: (a) holding time and (b) holding temperature, on the tensile strength of annealed AM Ti6Al4V. By the prediction result generated from the artificial neural network model.

coarser for higher holding temperatures, and the YS dropped from 1110 ± 9 MPa to 760 ± 19 MPa after the sample was annealed at 1020°C , followed by furnace cooling.

In the classic theory, Hall-Petch relationship as shown in Eq. (14) was widely used to describe the yield strength (σ_Y), in order to capture the effect of microstructural morphologies (Labusch, 1970), as seen in Eq. (14):

$$\sigma_Y = \sigma_0 + \frac{k_{\text{HP}}}{\sqrt{D_\alpha}}, \quad (14)$$

where D_α is the mean grain size of α phase (in microns), k_{HP} is the Hall-Petch coefficient of a given material, and σ_0 is the friction stress that is the critical resolved shear stress to initiate slip in a grain. Galarraga *et al.* (2017) studied the heat-treatment influence on electron beam melting (EBM) samples and concluded that the σ_0 was 737 MPa and k_{HP} was $144 \text{ MPa } \mu\text{m}^{1/2}$. The Hall-Petch relationship predicts that the yield strength decreases as the α grain grows. As shown in Figure 6, a new relationship between predicted YS and α lath thickness of AM Ti6Al4V samples is established using the SLM and EBM data collected in this study. Figure 6 compares the reported YS and α lath thickness from the literature (purple and green points), the Hall-Petch prediction using the σ_0 and k_{HP} reported by Galarraga *et al.* (2017) (black line), the Hall-Petch prediction with the new σ_0 and k_{HP} , obtained by fitting the YS and α lath thickness data in our database for AM Ti6Al4V (blue dot line), and the prediction by the established ANN model (red line). The ANN model predicted that when the α lath thickness increases from 0.7 to 3.4 μm , the yield strength decreases from 966 to 868 MPa. The new Hall-Petch prediction (blue dotted line) agrees well with the ANN prediction (red line). By fitting the collected SLM and EBM data with the Hall-Petch equation, a new σ_0 of 767 MPa, which is very close to that of Galarraga's study, and a new k_{HP} of $191 \text{ MPa } \mu\text{m}^{1/2}$, which is significantly larger than that of the Galarraga's study, were found, as shown in Eq. (15):

$$\sigma_Y = 767 \text{ MPa} + \frac{191 \text{ MPa} + \mu\text{m}^{1/2}}{\sqrt{D_\alpha}}, \quad (15)$$

where D_α is the mean grain size of α phase (in microns). The differences in the Hall-Petch coefficients obtained in this study and in the Galarraga *et al.*'s study (Galindo-Fernández *et al.*, 2018) may be related to the very long exposure time (20–170 h) used in Galarraga *et al.*'s heat-treatment process. It is known that a long heat-treatment period reduces the dislocation pile-up and results in a softening effect. Another possible cause of the Hall-Petch coefficient difference is the difference in composition. The material used in Galarraga *et al.*'s study was Ti6Al4V ELI with very low level of impurities such as Fe and O, in comparison with Ti6Al4V (Salmi *et al.*, 2012). This difference in alloy composition may have contributed to the decrease in tensile strength (the Hall-Petch coefficient) but increase in failure strain. Even though previous studies showed that there was a notable difference in the microstructure of Ti6Al4V parts produced by SLM and EBM (Rafi *et al.*, 2013), Figure 6 suggests that the new Hall-Petch equation can be used for post-annealing Ti6Al4V parts produced by both the SLM and EBM processes. However, the Hall-Petch equation only considers the mean grain size of α phase (in microns). The volume fraction of α , Feret diameter of α , solid solution strengthening effect, etc., are factors that could also influence the yield strength (Galindo-Fernández *et al.*, 2018; Masuo *et al.*, 2018). These factors may be worth consideration in future studies.

According to the ASTM standard (Standard Specification for Wrought Titanium-6Aluminum-4Vanadium Extra Low Interstitial) for Surgical Implant Applications (UNS R56401), the requirement of YS for Ti6Al4V is 795 MPa (ASTM, F, 2013). Overall, the ANN result suggests that an annealing process of the holding time of fewer than 4 h and the holding temperature lower than 850°C is desirable for as-printed Ti6Al4V parts to reach the YS required by this standard.

The mechanical properties of as-printed samples showed a strong influence on post-annealing properties, as seen in Figure 7. The table in Figure 7 summarizes the six groups of data used as inputs to the model to generate the predicted YS in this figure. The data groups were selected so that the elongation inputs were from 2% to 12%, with a 2% step. The temperatures were selected according to 25 percentile, 50 percentile, and 75 percentile of the annealing holding temperature, as shown in Table 2. In addition, the holding times were randomly chosen as between

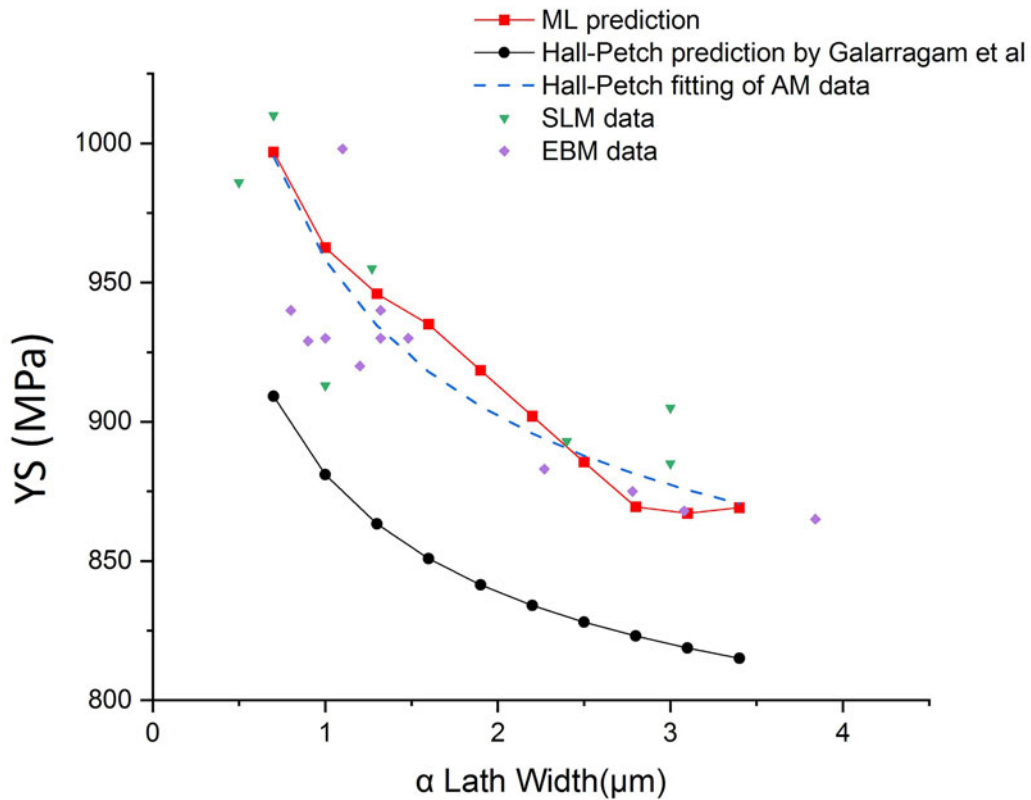


Fig. 6. The influence of a lath thickness of heat-treated sample on the yield strength of heat-treated AM Ti6Al4V by the prediction result generated from the artificial neural network model.

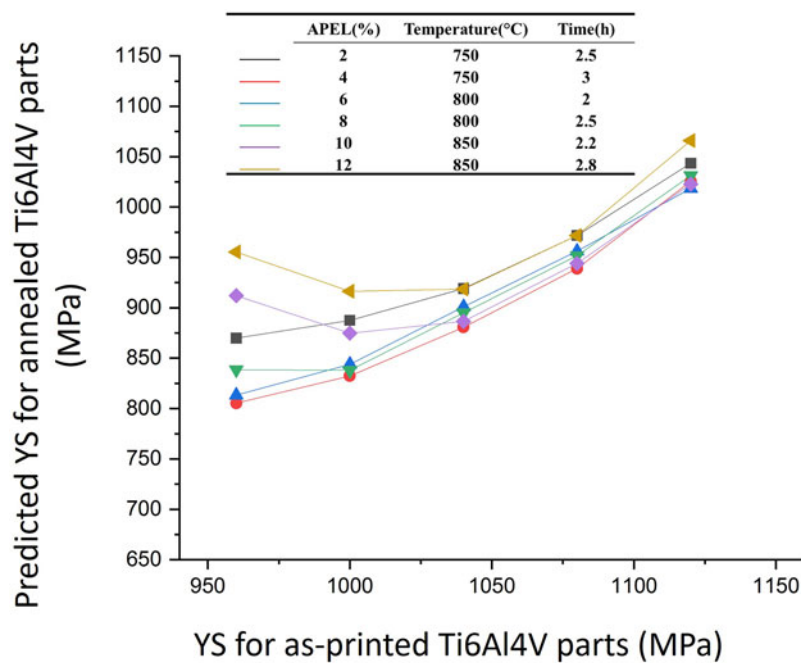


Fig. 7. The influence of mechanical properties of as-fabricated sample: yield strength (YS), on the yield strength of annealed AM Ti6Al4V.

2 and 3 h, since most reported studies had holding time within this range. As seen in Figure 7, in general, the YS of annealed Ti6Al4V parts increases with the increase in the YS of as-printed parts. It is well recognized that the annealing process cannot

remove the porosity in as-printed samples, which means that the defects remain after the annealing process. As a result, the printing quality strongly influences the quality and mechanical properties of post-annealing samples, and the mechanical

properties of as-printed sample is recognized as a strong influential factor for annealed final products.

Ultimate tensile strength

The error and the prediction accuracy of the established ANN model for UTS are shown in Figure 8. As seen in Figure 8a,b, the reduction of MAE and MSE in the UTS prediction are similar to that in the prediction of YS. The MAE after the learning process was found to be 35.5 MPa, and the accuracy number was 96.6%. The prediction results show a high accuracy with 88.6% of the prediction results within the 5% error range, as seen in Figure 8c,d. The prediction of UTS as a function of annealing time, holding temperature, and initial UTS, are summarized in Figures 8 and 9. The tables in Figure 9a,b summarize the six groups of data used for results shown in Figure 9a,b, respectively. Again, three groups of inputs were selected according to 25 percentile, 50 percentile, and 75 percentile data range of APYS, APTS, and APEL in Table 2, and the other three groups were randomly selected. As shown in Figure 9a, the UTS decreased with increase in holding time. It dropped from 933–1098 MPa to 861–975 MPa when the holding time increased from 1 to 4 h for all six scenarios in table in Figure 9a. The UTS decreased with the increase in holding temperature. UTS decreased from 1035–1220 MPa to 810–1129 MPa when the annealing temperature increased from 650°C to 1000°C in all six scenarios in table in Figure 9b. This trend is similar to that of YS (as discussed

previously). Thus, holding time and temperature are identified as strong influencing factors of UTS in annealing.

The table in Figure 10 summarizes the inputs used to obtain the results in Figure 10. As shown in Figure 10, in general the UTS of annealed Ti6Al4V parts increases with the increase in the UTS of as-printed parts, similar to the observation obtained in YS. Thus, it is concluded that the initial UTS has a strong influence on annealed UTS for SLM Ti6Al4V parts.

Elongation

The error and the prediction accuracy of the established ANN model for elongation (EL) are shown in Figure 11. In general, the prediction of EL shows relatively low accuracy when compared with the prediction of YS and UTS. Although the MAE of the training set approached 0% when the iteration reached 1000 epochs, the validation error was around 2%, as shown in Figure 11a,b. The MAE for the whole dataset was found to be 0.82%, and the accuracy number was 90.56%. As shown in Figure 11c,d, 86% of prediction results were within 15% error range. The prediction accuracy of EL is lower than those for YS and UTS. As discussed previously, grain size has a significant effect on the YS and UTS of the annealed Ti6Al4V. The grain size is influenced by the microstructure of the as-printed material and heat-treatment process parameters. However, the defects, especially porosity, are widely reported as important factors in determining elongation in as-printed Ti6Al4V parts prepared

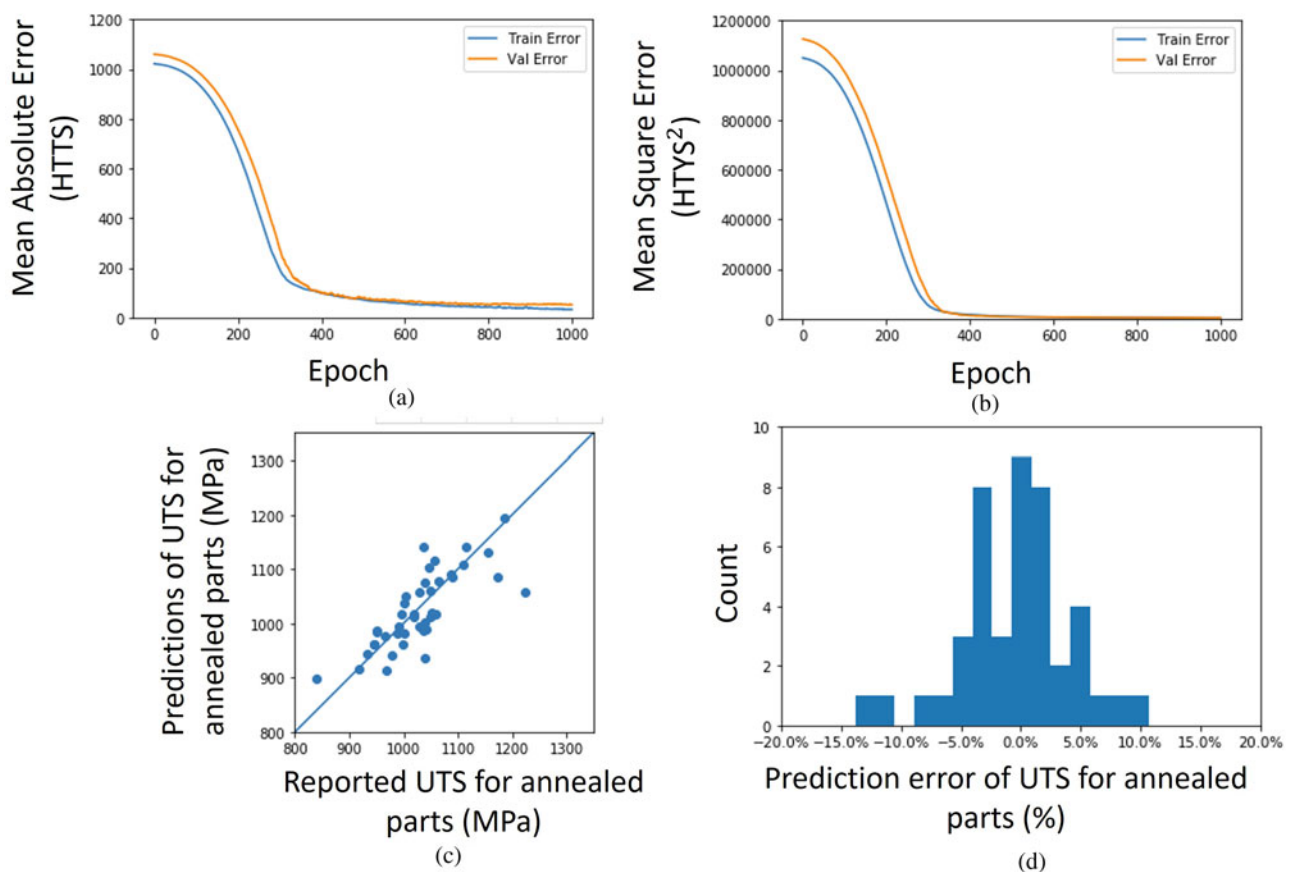


Fig. 8. Prediction of ultimate tensile strength (UTS) of annealed parts (a) mean absolute error (MAE) and (b) mean square error in the training process for predicting yield strength of annealed AM Ti6Al4V. (c) The correlation of the reported and predicted UTS values of annealed AM Ti6Al4V. (d) The distribution for UTS prediction error in each error range of annealed Ti6Al4V.

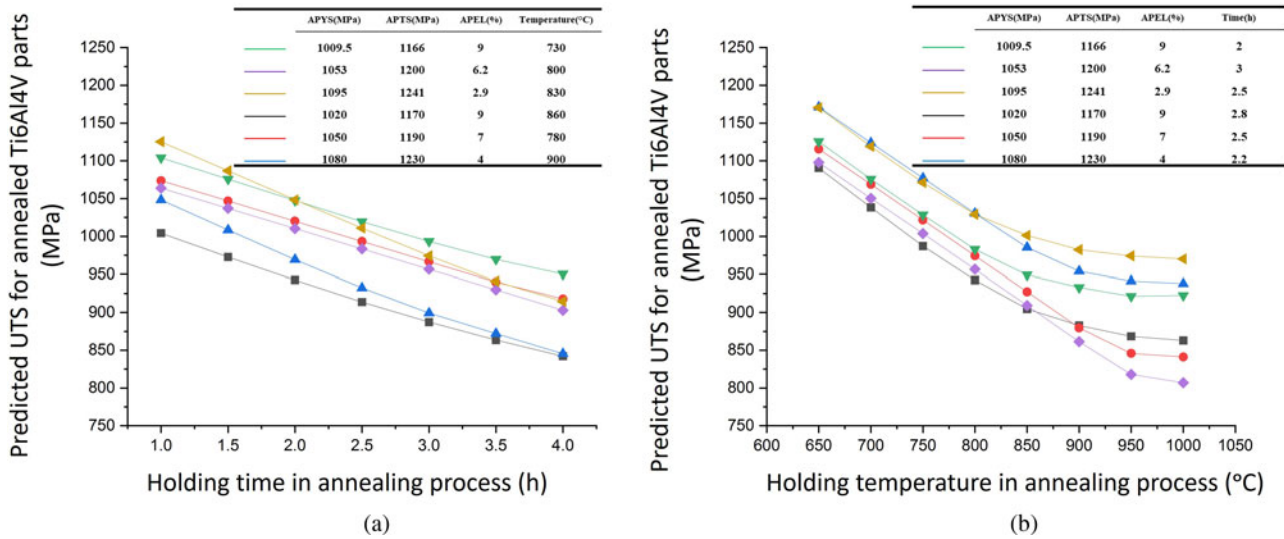


Fig. 9. The influence of heat treatment parameters: (a) holding time and (b) holding temperature, on UTS of annealed AM Ti6Al4V. By the prediction result generated from the artificial neural network model.

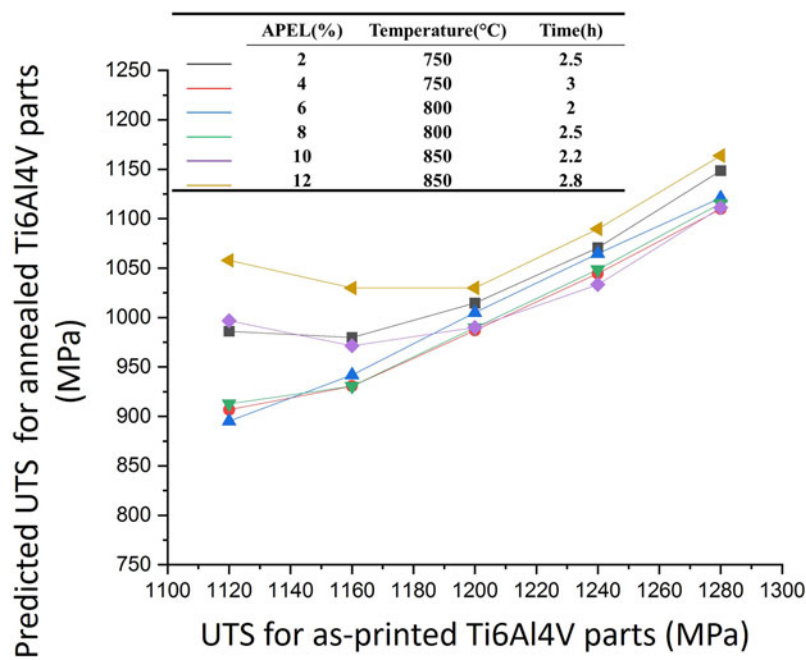


Fig. 10. The influence of mechanical properties of as fabricated sample: UTS, on the tensile strength of annealed AM Ti6Al4V by the prediction result generated from the artificial neural network model.

by the SLM process (Vilaro *et al.*, 2011; Luo *et al.*, 2015; Zhao *et al.*, 2016; Cao *et al.*, 2018; Romero *et al.*, 2018; Fatemi *et al.*, 2019). There are two main mechanisms that result in porosity in as-printed SLM Ti6Al4V parts: the lack of fusion of the melting pool (Liu *et al.*, 2014) and entrapped gas among Ti6Al4V powders (Gong *et al.*, 2015). The porosity accelerates the propagation of cracks and diminishes elongation at failure (Vilaro *et al.*, 2011; Clark *et al.*, 2012). The porosity introduced in the printing process could be very different from machine to machine and process to process. Moreover, the orientation of elongation in laser-processed Ti6Al4V may differ, due to the change in printing direction (Cao *et al.*, 2017). It has been shown that the annealing process has limited effect on removing or changing porosities

(Yan *et al.*, 2018). However, the annealing can significantly change the microstructure around defects and change the behavior of defects in failure. It was difficult to find sufficient data on defects to include in the database used in this study. Thus, the model lacks information to develop an accurate prediction on elongation. These factors can each contribute to large scattering of the elongation data in the dataset used in this study, and, thus, result in low prediction accuracy for elongation. In order to understand the role of defects in failure, a microstructure image-based, deep learning method may be needed to create a model that can directly factor in the influence of volume fraction, shape, and the distribution of defects on elongation of Ti6Al4V. As shown in Figure 12, three groups of the data were used as

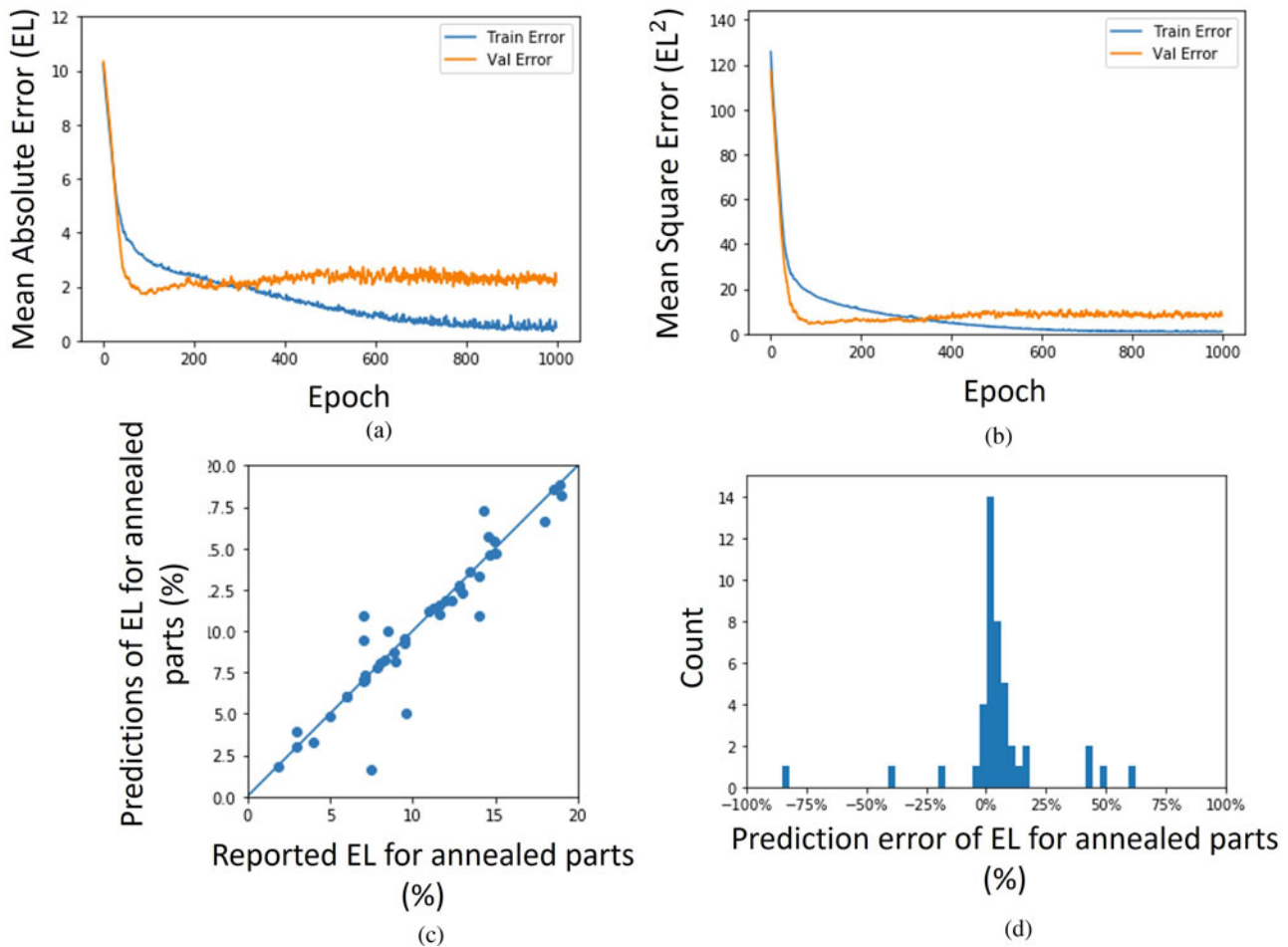


Fig. 11. Prediction of elongation (EL) of annealed parts (a) mean absolute error (MAE) and (b) mean square error in the training process for predicting EL of annealed AM Ti6Al4V. (c) The correlation of the reported and predicted EL values of annealed AM Ti6Al4V. (d) The distribution for EL prediction error in each range of annealed Ti6Al4V.

inputs, to reveal the influence of holding time on the predicted EL of heat-treated parts. The data of the three groups used here was the same with the second, third, and fourth groups of data in table for Figure 5, because they have similar holding temperatures. In Figure 12, it was observed that there were large variations in the predicted elongation of the annealed parts, even with similar heat-treatment parameters (holding time and temperature). This may be also attributed to the large scattering of elongation data in the database.

Figure 13 shows a plot of raw data used in the ANN modeling for EL. The black points represent EL of as-printed parts in the x -axis and EL of annealed Ti6Al4V parts in the y -axis. It can be observed that there is a larger scattering of EL data for both as-printed and heat-treated samples. The printing quality may have played an important role in the observed large variation of elongation in the as-printed parts. Voisin *et al.* (2018) found that a small volume ratio of porosity resulted in low failure strain in as-printed samples. They concluded that the nucleation and growth could have reduced the failure strain. Yan *et al.* (2020) observed large insufficiently fused areas in as-printed SLM Ti6Al4V, which led to low failure strain. The experimental data in this study were collected from reports using a variety of printers and printing procedures. This difference could result in different structural defects in the samples in these reports and lead

to a large scattering of the elongation in as-printed samples. Linear regression of all the elongation data resulted in a general increasing trend, represented by the red line in Figure 13. The blue dotted line indicates that the elongation for annealed Ti6Al4V parts is equal to the elongation for the as-printed sample. Most of the collected data are located above the blue dotted line. This observation suggests that the annealing treatment indeed improves elongation in general. It was shown that the annealing treatment could change the microstructure of as-printed Ti6Al4V samples from martensite to a ductile lamellar $\alpha+\beta$ and result in improvement of elongation (Yadroitsev *et al.*, 2014). But the annealing process cannot close the defects, and the defects still have a significant influence on elongation of annealed parts.

Conclusion

In this research, an ANN model was built to predict the mechanical properties, including YS, UTS, and EL, of annealed Ti6Al4V prepared by SLM. The model exhibited a high accuracy in prediction YS and UTS. For YS prediction, 88.6% of prediction results were within 5% error range, and the accuracy number was 96.7%. For UTS prediction, 88.6% of prediction results were within 5% error range, and the accuracy number was 96.6%.

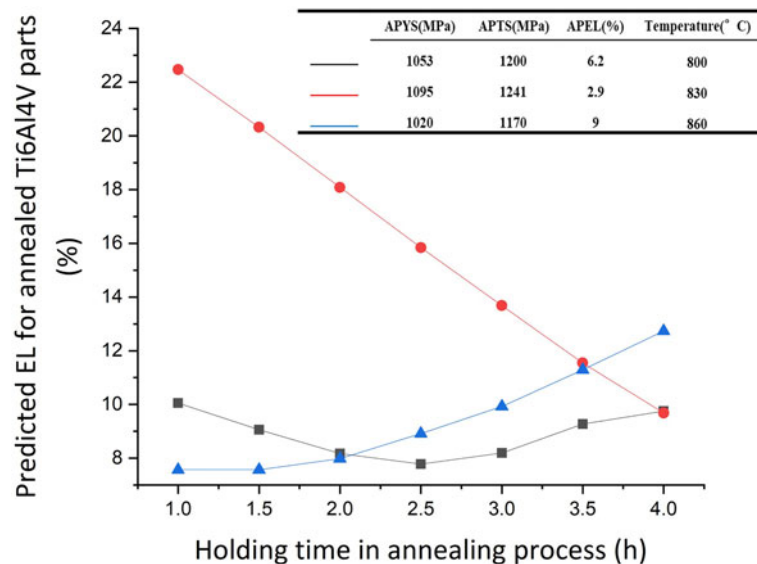


Fig. 12. The influence of holding time on EL of annealed AM Ti6Al4V by the prediction result generated from the artificial neural network model.

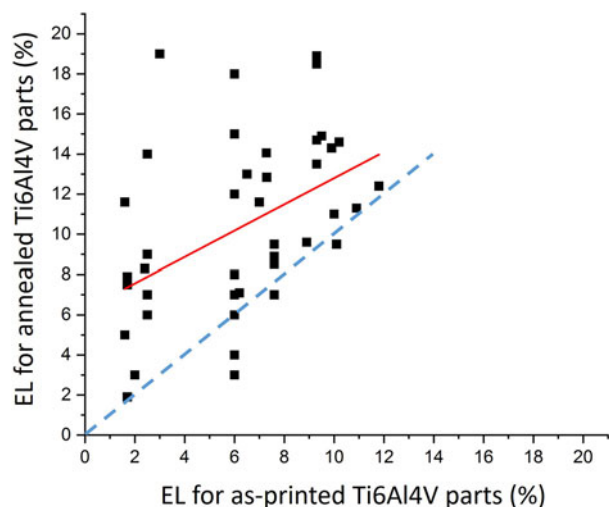


Fig. 13. Summary of reported elongation data: elongation of annealed Ti6Al4V as a function of elongation in as-printed Ti6Al4V.

The established model was then used to reveal the relationship between the mechanical properties of final parts and various inputs, including initial mechanical properties and heat-treatment parameters. The model showed that the final YS and UTS after annealing were sensitive to annealing temperature and holding time. A new Hall-Petch relationship with $\sigma_0 = 767$ MPa and $k_{HP} = 191$ MPa $\mu\text{m}^{1/2}$ was proposed for AM Ti6Al4V parts after annealing. It was found that the YS and UTS were also sensitive to properties of the as-printed Ti6Al4V, since the annealing process could not effectively remove defects in the as-printed samples. The prediction of EL showed relatively low accuracy compared with that of YS and UTS. The MAE for the whole dataset was found to be 0.82%, and the accuracy number was 90.56%. There were large variations in predicted elongation of the annealed parts, even with similar heat-treatment parameters. This was attributed to the difference in printers and printing conditions used in the many studies that provided data for the current model. Differences in printing processes may have resulted in different structural defects in the samples studied in these reports

and led to a large scattering of the elongation data. These results indicate that optimizing the printing process to reduce the defects and improve the overall mechanical properties for as-printed parts is desirable in order to achieve good mechanical properties in annealed Ti6Al4V parts prepared by the AM process.

References

- Ahmed T and Rack H (1998) Phase transformations during cooling in $\alpha+\beta$ titanium alloys. *Materials Science and Engineering: A* **243**, 206–211.
- Alam M (2020) Data Normalization in Machine Learning. Available at: <https://towardsdatascience.com/data-normalization-in-machine-learning-395fdec69d02>.
- Alpaydin E (2020) *Introduction to Machine Learning*. Cambridge, MA: MIT Press.
- ASTM F (2013) Standard Specification for Wrought Titanium-6Aluminum-4Vanadium ELI (Extra Low Interstitial) Alloy for Surgical Implant Applications (UNS R56401). ASTM F136-13.
- Banerjee D and Williams J (2013) Perspectives on titanium science and technology. *Acta Materialia* **61**, 844–879.
- Barriobero-Vila P, et al. (2017) Inducing stable $\alpha+\beta$ microstructures during selective laser melting of Ti-6Al-4V using intensified intrinsic heat treatments. *Materials* **10**, 268.
- Bilgin GM, et al. (2017) Optimization of the mechanical properties of Ti-6Al-4V alloy fabricated by selective laser melting using thermohydrogen processes. *Materials Science and Engineering: A* **700**, 574–582.
- Cao S, et al. (2017) Defect, microstructure, and mechanical property of Ti-6Al-4V alloy fabricated by high-power selective laser melting. *JOM* **69**, 2684–2692.
- Cao F, et al. (2018) A review of the fatigue properties of additively manufactured Ti-6Al-4V. *JOM* **70**, 349–357.
- Carpenter Technical Datasheet Titanium Alloy Ti 6Al-4V, by Carpenter Technology. Available at: <https://www.carpentertechnology.com/hubfs/7407324/Material%20Safety%20Data%20Sheets/Ti%206Al-4V.pdf> (accessed 12 September 2021).
- Clark D, Whittaker MT and Bache MR (2012) Microstructural characterization of a prototype titanium alloy structure processed via direct laser deposition (DLD). *Metallurgical and Materials Transactions B* **43**, 388–396.
- Donachie MJ (2000) *Titanium: A Technical Guide*. Materials Park, OH: ASM International.
- Ducato A, et al. (2013) An automated visual inspection system for the classification of the phases of Ti-6Al-4V titanium alloy. In *International Conference on Computer Analysis of Images and Patterns*. Springer.

- Ettefagh AH, et al.** (2019) Corrosion behavior of additively manufactured Ti-6Al-4V parts and the effect of post annealing. *Additive Manufacturing* **28**, 252–258.
- Fatemi A, et al.** (2019) Fatigue behaviour of additive manufactured materials: an overview of some recent experimental studies on Ti-6Al-4V considering various processing and loading direction effects. *Fatigue & Fracture of Engineering Materials & Structures* **42**, 991–1009.
- Frazier WE** (2014) Metal additive manufacturing: a review. *Journal of Materials Engineering and Performance* **23**, 1917–1928.
- Galarraga H, et al.** (2017) Effects of heat treatments on microstructure and properties of Ti-6Al-4V ELI alloy fabricated by electron beam melting (EBM). *Materials Science and Engineering: A* **685**, 417–428.
- Galindo-Fernández M, et al.** (2018) A microstructure sensitive model for deformation of Ti-6Al-4V describing cast-and-wrought and additive manufacturing morphologies. *Materials & Design* **160**, 350–362.
- Gandhi R** (2018) A Look at Gradient Descent and RMSprop Optimizers. Available from: <https://towardsdatascience.com/a-look-at-gradient-descent-and-rmsprop-optimizers-f77d483ef08b>.
- Ghamarian I, et al.** (2016) Developing a phenomenological equation to predict yield strength from composition and microstructure in β processed Ti-6Al-4V. *Materials Science and Engineering: A* **660**, 172–180.
- Glavicic M and Venkatesh V** (2014) Integrated computational materials engineering of titanium: current capabilities being developed under the metals affordability initiative. *JOM* **66**, 1310–1320.
- Gong H, et al.** (2015) Influence of defects on mechanical properties of Ti-6Al-4V components produced by selective laser melting and electron beam melting. *Materials & Design* **86**, 545–554.
- Hayes BJ, et al.** (2017) Predicting tensile properties of Ti-6Al-4V produced via directed energy deposition. *Acta Materialia* **133**, 120–133.
- Herzog D, et al.** (2016) Additive manufacturing of metals. *Acta Materialia* **117**, 371–392.
- Huang Q, et al.** (2016) Microstructure and inclusion of Ti-6Al-4V fabricated by selective laser melting. *Frontiers of Materials Science* **10**, 428–431.
- Kar S, et al.** (2006) Modeling the tensile properties in β -processed α/β Ti alloys. *Metallurgical and Materials Transactions A* **37**, 559–566.
- Katzarov I, Malinov S and Sha W** (2002) Finite element modeling of the morphology of β to α phase transformation in Ti-6Al-4V alloy. *Metallurgical and Materials Transactions A* **33**, 1027–1040.
- Kumar P, Prakash O and Ramamurty U** (2018) Micro- and meso-structures and their influence on mechanical properties of selectively laser melted Ti-6Al-4V. *Acta Materialia* **154**, 246–260.
- Labusch R** (1970) A statistical theory of solid solution hardening. *Physica Status Solidi (b)* **41**, 659–669.
- Lin J, et al.** (2017) Microstructural evolution and mechanical property of Ti-6Al-4V wall deposited by continuous plasma arc additive manufacturing without post heat treatment. *Journal of the Mechanical Behavior of Biomedical Materials* **69**, 19–29.
- Liu QC, et al.** (2014) The effect of manufacturing defects on the fatigue behaviour of Ti-6Al-4V specimens fabricated using selective laser melting. In *Advanced Materials Research*. Trans Tech Publ. Vol. 891, pp. 1519–1524.
- Luo SD, et al.** (2010) Microwave sintering of titanium. In *Key Engineering Materials*. Trans Tech Publ. Vol. **436**, pp. 141–147.
- Luo SD, Qian M and Imam MA** (2015) Microwave sintering of titanium and titanium alloys. In *Titanium Powder Metallurgy*. Elsevier, pp. 237–251.
- Malinov S, Sha W and McKeown J** (2001) Modelling the correlation between processing parameters and properties in titanium alloys using artificial neural network. *Computational Materials Science* **21**, 375–394.
- Masuo H, et al.** (2018) Influence of defects, surface roughness and HIP on the fatigue strength of Ti-6Al-4V manufactured by additive manufacturing. *International Journal of Fatigue* **117**, 163–179.
- Parry L, Ashcroft I and Wildman RD** (2016) Understanding the effect of laser scan strategy on residual stress in selective laser melting through thermo-mechanical simulation. *Additive Manufacturing* **12**, 1–15.
- Qian M** (2010) Cold compaction and sintering of titanium and its alloys for near-net-shape or preform fabrication. *International Journal of Powder Metallurgy* **46**, 29–44.
- Qian M, et al.** (2016) Additive manufacturing and postprocessing of Ti-6Al-4V for superior mechanical properties. *MRS Bulletin* **41**, 775–784.
- Rafi H, et al.** (2013) Microstructures and mechanical properties of Ti6Al4V parts fabricated by selective laser melting and electron beam melting. *Journal of Materials Engineering and Performance* **22**, 3872–3883.
- Romero C, Yang F and Bolzoni L** (2018) Fatigue and fracture properties of Ti alloys from powder-based processes—a review. *International Journal of Fatigue* **117**, 407–419.
- Salmi M, et al.** (2012) Patient-specific reconstruction with 3D modeling and DMLS additive manufacturing. *Rapid Prototyping Journal* **18**, 209–214.
- Semiatin S, et al.** (2003) Microstructure evolution during alpha-beta heat treatment of Ti-6Al-4V. *Metallurgical and Materials Transactions A* **34**, 2377–2386.
- Semiatin S, Stefansson N and Doherty R** (2005) Prediction of the kinetics of static globularization of Ti-6Al-4V. *Metallurgical and Materials Transactions A* **36**, 1372–1376.
- Shi X, et al.** (2015) Microstructure-tensile properties correlation for the Ti-6Al-4V titanium alloy. *Journal of Materials Engineering and Performance* **24**, 1754–1762.
- Simonelli M, Tse YY and Tuck C** (2012) Microstructure of Ti-6Al-4V produced by selective laser melting. *Journal of Physics: Conference Series*. Vol. 371, No. 1, p. 012084.
- Simonelli M, Tse YY and Tuck C** (2014) Effect of the build orientation on the mechanical properties and fracture modes of SLM Ti-6Al-4V. *Materials Science and Engineering: A* **616**, 1–11.
- Stefansson N, Semiatin S and Eylon D** (2002) The kinetics of static globularization of Ti-6Al-4V. *Metallurgical and Materials Transactions A* **33**, 3527–3534.
- Tamilselvi S, Raman V and Rajendran N** (2006) Corrosion behaviour of Ti-6Al-7Nb and Ti-6Al-4 V ELI alloys in the simulated body fluid solution by electrochemical impedance spectroscopy. *Electrochimica Acta* **52**, 839–846.
- Ter Haar GM and Becker TH** (2018) Selective laser melting produced Ti-6Al-4V: post-process heat treatments to achieve superior tensile properties. *Materials* **11**, 146.
- Theodoridis S** (2015) *Machine Learning: A Bayesian and Optimization Perspective*. Cambridge, MA: Academic Press.
- Tirelli S, et al.** (2015) Economical comparison of cryogenic vs. traditional turning of Ti-6Al-4V: a case study. In *Key Engineering Materials*. Trans Tech Publ Vol. **651**, pp. 1204–1210.
- Vilaro T, Colin C and Bartout J-D** (2011) As-fabricated and heat-treated microstructures of the Ti-6Al-4V alloy processed by selective laser melting. *Metallurgical and Materials Transactions A* **42**, 3190–3199.
- Voisin T, et al.** (2018) Defects-dictated tensile properties of selective laser melted Ti-6Al-4V. *Materials & Design* **158**, 113–126.
- Vrancken B, et al.** (2012) Heat treatment of Ti6Al4V produced by selective laser melting: microstructure and mechanical properties. *Journal of Alloys and Compounds* **541**, 177–185.
- Wang M, et al.** (2016) Fabrication and characterization of selective laser melting printed Ti-6Al-4 V alloys subjected to heat treatment for customized implants design. *Progress in Natural Science: Materials International* **26**, 671–677.
- Xu Y, et al.** (2017) Effect of annealing treatments on the microstructure, mechanical properties and corrosion behavior of direct metal laser sintered Ti-6Al-4V. *Journal of Materials Engineering and Performance* **26**, 2572–2582.
- Yadroitsava I, et al.** (2015) Residual stress in SLM Ti6Al4V alloy specimens. In *Materials Science Forum*. Trans Tech Publ. Vol. 828, pp. 305–310.
- Yadroitsev I and Yadroitsava I** (2015) Evaluation of residual stress in stainless steel 316L and Ti6Al4V samples produced by selective laser melting. *Virtual and Physical Prototyping* **10**, 67–76.
- Yadroitsev I, Krakhmalev P and Yadroitsava I** (2014) Selective laser melting of Ti6Al4V alloy for biomedical applications: temperature monitoring and microstructural evolution. *Journal of Alloys and Compounds* **583**, 404–409.
- Yan X, et al.** (2018) Effect of heat treatment on the phase transformation and mechanical properties of Ti6Al4V fabricated by selective laser melting. *Journal of Alloys and Compounds* **764**, 1056–1071.
- Yan Q, et al.** (2020) Comparison study on microstructure and mechanical properties of Ti-6Al-4V alloys fabricated by powder-based selective-laser-melting and sintering methods. *Materials Characterization* **164**, 110358.

Zhao X, et al. (2016) Comparison of the microstructures and mechanical properties of Ti-6Al-4 V fabricated by selective laser melting and electron beam melting. *Materials & Design* **95**, 21–31.

Dr. Zhaotong Yang's research focuses on machine learning and deep learning-enabled exploration in material science and manufacturing engineering. He has developed machine learning and deep learning models to understand properties of Ti6Al4V parts prepared by additive manufacturing (AM), investigated using convolutional neural networks (CNN) to efficiently classify images of e-waste to reduce the labor cost and improve recycling efficiency, and improved the ceramic robocasting AM tool by establishing a close-loop control system with a machine learning model. Dr. Yang is passionate about effectively applying machine learning and deep learning methods to solve many pressing issues in the material and manufacturing engineering field.

Dr. Mei Yang is currently working at Wyman Gordon Grafton as a Principal Metallurgist following her position as Assistant Research Professor and Associate Technical Director of the Center for Heat Treating Excellence (CHTE) at Worcester Polytechnic Institute (WPI). Before joining WPI, she worked on refractory alloys as a Senior R&D Engineer at H.C. Starck. Her expertise is in integrated materials and processes development for both metals and ceramics by combining modeling and experimental investigation.

Professor Richard Sisson's main research interest is the application of diffusion and thermodynamics to the solution of materials problems. He is

currently working on modeling the surface treating of steels and the post processing of additively manufactured ceramics and metals. He has also worked on the effects of deposition process parameters on the microstructure and cyclic thermal stability of partially stabilized zirconia thermal barrier coatings. His research work has resulted in over three hundred publications and over three hundred technical presentations.

Professor Yanhua Li received two Ph.D. degrees in computer science from the University of Minnesota at Twin Cities in 2013 and in electrical engineering from the Beijing University of Posts and Telecommunications in China in 2009, respectively. He is currently an Associate Professor in the Department of Computer Science at Worcester Polytechnic Institute (WPI) in Worcester, MA. Prior to this, he worked in Bell Labs in New Jersey, and Microsoft Research Asia in Beijing. His research interests are big data analytics and artificial intelligence in many contexts, including urban intelligence, smart cities, and urban planning and optimization. He is a recipient of NSF CAREER award and NSF CRII award.

Professor Jianyu Liang is a Professor of Mechanical and Materials Engineering, with affiliated appointments in the Departments of Civil and Environmental Engineering, Chemical Engineering, and Fire Protection Engineering. Her research work on nanomaterials, additive manufacturing, agile manufacturing, machine learning for materials science and manufacturing engineering, and sustainability has been funded by NSF, NASA, DoD, ED, and industry. Her work has resulted in over 300 research papers and technical presentations. As an educator, Liang strives to equip students with the confidence, enthusiasm, knowledge, and skills to allow them to enjoy learning throughout their lives.